Inorganic Chemistry

Article

pubs.acs.org/IC

The Role of Connectivity on Electronic Properties of Lead Iodide Perovskite-Derived Compounds

Machteld E. Kamminga,[†] Gilles A. de Wijs,[‡] Remco W. A. Havenith,[†,§,⊥] Graeme R. Blake,[†] and Thomas T.M. Palstra*[,†,∥]

[†]Zernike Institute for Advanced Materials and [§]Stratingh Institute for Chemistry, University of Groningen, Nijenborgh 4, 9747 AG Groningen, The Netherlands

[‡]Radboud University, Institute for Molecules and Materials, Heyendaalseweg 135, 6525 AJ Nijmegen, The Netherlands

[⊥]Ghent Quantum Chemistry Group, Department of Inorganic and Physical Chemistry, Ghent University, Krijgslaan 281 (S33), B-9000 Gent, Belgium

Supporting Information

ABSTRACT: We use a layered solution crystal growth method to synthesize high-quality single crystals of two different benzylammonium lead iodide perovskite-like organic/inorganic hybrids. The well-known $(C_6H_5CH_2NH_3)_2PbI_4$ phase is obtained in the form of bright orange platelets, with a structure comprised of single ⟨100⟩-terminated sheets of corner-sharing PbI_6 octahedra separated by bilayers of the organic cations. The presence of water during synthesis leads to formation of a novel minority phase that crystallizes in the form of nearly transparent, light yellow bar-shaped crystals. This phase adopts the monoclinic space group $P2_1/n$ and incorporates water molecules, with structural formula $(C_6H_5CH_2NH_3)_4Pb_5I_{14}{\cdot}2H_2O$. The crystal structure consists of ribbons of edge-sharing PbI_6 octahedra separated by the organic cations. Density functional theory calculations including spin−orbit coupling show that these edge-sharing PbI_6 octahedra cause the band gap to increase with respect to corner-sharing PbI_6 octahedra in $(C_6H_5CH_2NH_3)_2PbI_4$. To gain systematic insight, we model the effect of the connectivity of PbI_6 octahedra on the band gap in idealized lead iodide perovskite-derived compounds. We find that increasing the connectivity from corner-, via edge-, to face-sharing causes a significant increase in the band gap. This provides a new mechanism to tailor the optical properties in organic/inorganic hybrid compounds.

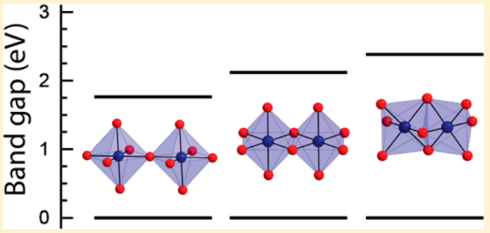

INTRODUCTION

Organic/inorganic hybrid perovskites have attracted growing attention for optoelectronic applications such as light-emitting diodes,[1,2] lasers,[3,4] photodetectors,[5] and efficient planar heterojunction solar cell devices.[6−10] Besides having unique optical[11,12] and excitonic[13,14] properties, they are easy to synthesize. While very high power-conversion efficiencies of up to 22.1% have been reported for lead iodide-based solar cells,[15] various challenges remain. One of these challenges is to improve resilience to ambient conditions, including moisture: it affects the morphology of the organic/inorganic hybrid perovskite layer, and low-quality perovskite films can have pinholes that create shunting pathways that drastically limit the device performance.

Recently, Conings et al. studied the influence of water contamination in organometal halide perovskite precursors on the resulting perovskite film and solar cells.[16] Their results suggest that water has no considerable influence on the photovoltaic performance of devices. Moreover, other studies have shown that moisture during film growth is of importance to enhance the formation and quality of the hybrid perovskite films, as well as their photoluminescence (PL) performance.[17,18] Furthermore, Eperon et al. used powder X-ray diffraction (XRD) to show that the expected $CH_3NH_3PbI_3$ phase forms even at high levels of humidity.[18] However, we show here that water can also have undesired effects. The presence of water during the synthesis of the two-dimensional (2D) compound $(C_6H_5CH_2NH_3)_2PbI_4$ yields small quantities of a second benzylammonium lead iodide phase with a larger band gap. This new compound has the structural formula $(C_6H_5CH_2NH_3)_4Pb_5I_{14}{\cdot}2H_2O$, with water incorporated into the crystal structure. The inorganic network consists of ribbons of edge-sharing PbI_6 octahedra. Previously, we showed that face-sharing PbI_6 octahedra exhibit an electronic confinement effect and force the band gap to increase.[19] Here, using density functional theory calculations with spin−orbit coupling (DFT+SOC), we study the electronic structure of $(C_6H_5CH_2NH_3)_4Pb_5I_{14}{\cdot}2H_2O$ and show how the charge distribution is affected when edge-sharing PbI_6 octahedra are introduced. Thus, we provide a design rule for tuning the optical properties of organic/inorganic hybrid materials based on the connectivity of the metal-halide octahedra. Notably, the class of organic/inorganic hybrid perovskite(-derived) materials

Received: May 1, 2017
Published: July 5, 2017

DOI: 10.1021/acs.inorgchem.7b01096
Inorg. Chem. 2017, 56, 8408−8414

have several structural features that influence the optical properties. These structural features include the choice of metal and halide (ionic radii) and rotations/deformations of the inorganic backbone. These factors not only influence the band gap directly but also each other and hence the band gap indirectly. Several studies have investigated the effect of structural deformations on the optical properties in great detail.[19−24] In our study, we focus on the effect that connectivity of metal-halide octahedra has on the band gap in lead iodide systems. We demonstrate that the size of the band gap strongly depends on not only the dimensionality of the inorganic network but also on the number of iodides shared between two adjacent lead ions, resulting in corner-, edge-, or face-sharing PbI_6 octahedra. We conclude that, counter-intuitively, the band gap increases with the number of shared iodides.

EXPERIMENTAL SECTION

Crystal Growth. Single crystals of $(C_6H_5CH_2NH_3)_2PbI_4$ and $(C_6H_5CH_2NH_3)_4Pb_5I_{14}\cdot 2H_2O$ were grown at room temperature using the same layered solution technique as used in our previous work.[19] PbI_2 (74 mg, 0.16 mmol; Sigma-Aldrich; 99%) was dissolved in 3.0 mL of concentrated (57 wt %) aqueous hydriodic acid (Sigma-Aldrich; 99,95%). Absolute methanol (3.0 mL; Lab-Scan; anhydrous, 99.8%) was carefully placed on top of the PbI_2/HI mixture, without mixing the solutions. A sharp interface was formed between the two layers due to the large difference in densities. Benzylamine (Sigma-Aldrich; 99%) was added in great excess by gently adding 15 droplets, using a glass pipet, on top of the methanol layer. The reaction mixtures were kept in a fume hood under ambient conditions. After 2 d, a small number of crystals started to form. The crystals were collected after two weeks by washing three times with diethyl ether (Avantor). A mixture of three types of crystals was obtained: *bright orange* platelets ($(C_6H_5CH_2NH_3)_2PbI_4$), *colorless* needles (an unidentified phase), and *nearly transparent, light yellow* bar-shaped crystals ($(C_6H_5CH_2NH_3)_4Pb_5I_{14}\cdot 2H_2O$). Figure S1 shows a photograph of all three types of crystals.

X-ray Diffraction. Single-crystal X-ray diffraction (XRD) measurements were performed using a Bruker D8 Venture diffractometer equipped with a Triumph monochromator and a Photon100 area detector, operating with Mo Kα radiation. A 0.3 mm nylon loop and cryo-oil were used to mount the crystals. The crystals were cooled with a nitrogen flow from an Oxford Cryosystems Cryostream Plus. Data processing was done using the Bruker Apex III software, the structure was solved using direct methods, and the SHELX97 software[25] was used for structure refinement.

Computational Methods. The calculations were performed within DFT[26] in the Perdew−Burke−Ernzerhof (PBE) generalized gradient approximation (GGA)[27] including relativistic SOC effects with the Vienna Ab initio Simulation Package (VASP)[28,29] using the projector augmented wave (PAW) method.[30,31] PAW data sets supplied with were used with a frozen 1s, 1s, [Kr]4d^{10}, and [Xe] core for C, N, I, and Pb, respectively. The calculations were performed using the experimental lattice parameters and atomic positions, except for the hydrogen atoms, which were optimized. Furthermore, the water molecules were left out. Structural models were rendered using VESTA.[32]

RESULTS AND DISCUSSION

High-quality single crystals of benzylammonium lead iodide organic/inorganic hybrids were obtained using the layered solution crystal growth method as described in the Experimental Section. We performed this synthesis under ambient conditions and used methanol and hydriodic acid (57 wt % in H_2O) as solvents. As a result, water was present during crystal growth. We identified three different phases after synthesis, which could easily be distinguished as bright orange platelets, very thin colorless needles, and slightly thicker pale yellow bar-shaped crystals (see Figure S1). The first two phases were abundantly present, whereas the pale yellow bar-shaped crystals were present only in small quantities. We identified the orange platelets as the known $(C_6H_5CH_2NH_3)_2PbI_4$ compound (space group *Pbca*), consisting of ⟨100⟩-terminated sheets of corner-sharing PbI_6 octahedra separated by bilayers of the organic cation.[19,33] The structure of the thin colorless needles could not be solved, because the crystal quality was very poor. However, the pale yellow bar-shaped crystals were of good crystal quality and represent a novel benzylammonium lead iodide phase, the focus of this work.

Here, we investigate the crystal and electronic structure of the light yellow bar-shaped crystals and compare them to $(C_6H_5CH_2NH_3)_2PbI_4$. Our single-crystal XRD measurements reveal that these crystals exhibit a completely different structure to the orange platelets and have the chemical formula $(C_6H_5CH_2NH_3)_4Pb_5I_{14}\cdot 2H_2O$. The crystallographic data are given in Table 1. Figure 1 shows the crystal structures of $(C_6H_5CH_2NH_3)_2PbI_4$ and $(C_6H_5CH_2NH_3)_4Pb_5I_{14}\cdot 2H_2O$. The asymmetric unit of $(C_6H_5CH_2NH_3)_4Pb_5I_{14}\cdot 2H_2O$, showing thermal ellipsoids, is given in Figure S2.

Table 1. Crystallographic Data of $(C_6H_5CH_2NH_3)_4Pb_5I_{14}\cdot 2H_2O$

$(C_6H_5CH_2NH_3)_4Pb_5I_{14}\cdot 2H_2O$	
temperature (K)	100(2)
formula	$C_{28}H_{44}N_4O_2Pb_5I_{14}$
formula weight (g/mol)	3281.34
crystal size (mm^3)	0.26 × 0.12 × 0.08
crystal color	very light yellow
crystal system	monoclinic
space group	$P2_1/n$ (No. 14)
symmetry	centrosymmetric
Z	2
D (calculated) (g/cm^3)	3.572
F(000)	2432
a (Å)	17.4978(9)
b (Å)	7.9050(4)
c (Å)	22.6393(12)
α (deg)	90.0
β (deg)	103.0544(19)
γ (deg)	90.0
volume (Å^3)	3050.5(3)
μ (mm^{-1})	20.102
min/max transmission	0.161/0.780
θ range (degrees)	3.17−36.30
index ranges	$-21 < h < 21$
	$-9 < k < 9$
	$-28 < l < 28$
data/restraints/parameters	6218/2/245
GOF on F^2	1.082
No. total reflections	75 145
No. unique reflections	6218
No. obs $F_o > 4\sigma(F_o)$	5307
R_1 [$F_o > 4\sigma(F_o)$]	0.0269
R_1 [all data]	0.0354
wR_2 [$F_o > 4\sigma(F_o)$]	0.0586
wR_2 [all data]	0.0617
largest peak and hole (e Å^{-3})	1.25 and −1.40

DOI: 10.1021/acs.inorgchem.7b01096
Inorg. Chem. 2017, 56, 8408−8414

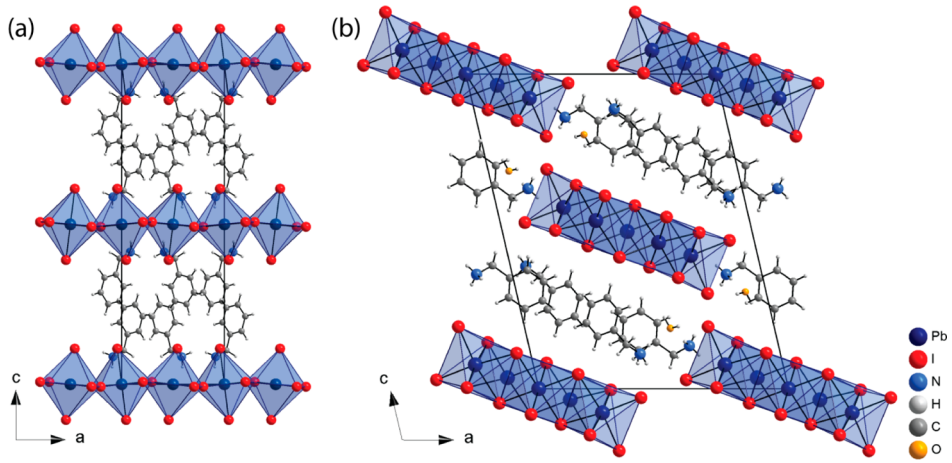

Figure 1. Polyhedral model of (a) $(C_6H_5CH_2NH_3)_2PbI_4$ and (b) $(C_6H_5CH_2NH_3)_4Pb_5I_{14}\cdot 2H_2O$ at 100 K, projected along the [010] direction. The H_2O molecules are rotationally disordered, and the orientation drawn should be considered illustrative only. Figure (a) is adapted from previous work.[19]

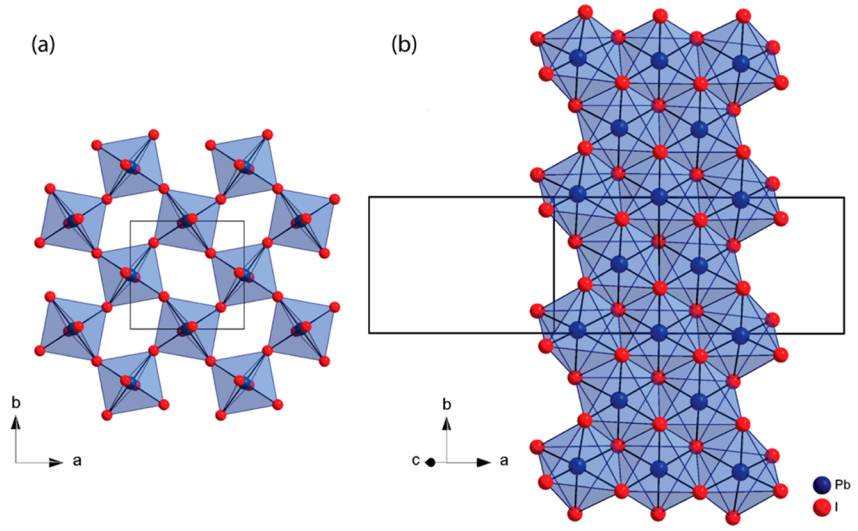

Figure 2. Polyhedral model of a single inorganic layer of (a) $(C_6H_5CH_2NH_3)_2PbI_4$ and (b) $(C_6H_5CH_2NH_3)_4Pb_5I_{14}\cdot 2H_2O$ at 100 K. (a) Projection along the [001] direction, where the corner-sharing PbI_6 octahedra form a slab that has translational symmetry along the *a*- and *b*-directions. Figure adapted from previous work.[19] (b) Projection perpendicular to the inorganic slabs, showing edge-sharing PbI_6 octahedra forming a $[Pb_5I_{14}]^{4-}$ ribbon with translational symmetry along the *b*-direction only.

As can be seen in Figure 1b, the crystal structure of $(C_6H_5CH_2NH_3)_4Pb_5I_{14}\cdot 2H_2O$ is rather different from its layered analogue. Despite consisting of the same building blocks, that is, benzylammonium and octahedrally coordinated lead iodide, $(C_6H_5CH_2NH_3)_4Pb_5I_{14}\cdot 2H_2O$ adopts an unusual structure. Whereas $(C_6H_5CH_2NH_3)_2PbI_4$ forms a 2D structure comprised of layers of corner-sharing PbI_6 octahedra, $(C_6H_5CH_2NH_3)_4Pb_5I_{14}\cdot 2H_2O$ forms a one-dimensional (1D) structure consisting of $[Pb_5I_{14}]^{4-}$ building blocks that form ribbons along the [010] direction. This is shown in Figure 2. Surprisingly, the connectivity in the inorganic part consists solely of edge-sharing PbI_6 octahedra. The starting compound, PbI_2, also consists of layers of edge-sharing PbI_6 octahedra. However, these layers are neutrally charged. In $(C_6H_5CH_2NH_3)_4Pb_5I_{14}\cdot 2H_2O$, these layers are cut into ribbons, giving rise to negatively charged $[Pb_5I_{14}]^{4-}$ building blocks. As a result, these ribbons are neutrally charged in their center and negatively charged at their edges, where the neutral PbI_2 pattern is broken. Therefore, the benzylammonium cations form hydrogen bonds with the outermost iodides of the inorganic ribbons. As a result, the phenyl rings are positioned between the inorganic ribbons. Notably, water molecules are also incorporated into the $(C_6H_5CH_2NH_3)_4Pb_5I_{14}\cdot 2H_2O$ crystal structure. After the inorganic backbone and the organic molecules were refined, using our single-crystal XRD data, a nonbonded center of electron density remained in a structural void. This intensity maximum closely matched the electron density of a water molecule, present during synthesis. Therefore, we conclude that water is incorporated in the crystal lattice. Thus, the presence of water during crystal growth induces the formation of an additional phase with completely different structural features and optical properties, as will be discussed below.

In our previous work, we studied the photoluminescence (PL) response and electronic structure of $(C_6H_5CH_2NH_3)_2PbI_4$ in more detail and found an experimental direct band gap of 2.12−2.19 eV in single crystals and a calculated direct band gap of 0.42 eV at the Γ point within DFT

DOI: 10.1021/acs.inorgchem.7b01096
Inorg. Chem. 2017, 56, 8408−8414

+SOC using the local density approximation (LDA).[19] We reason that this difference is likely due to the level of approximation employed and that incorporating quasiparticle corrections and excitonic effects would resolve the discrepancy. However, given the extended size of the unit cell, the inclusion of quasiparticle and electron−hole interaction effects is computationally prohibitive. For reference, in the case of $CH_3NH_3PbI_3$ quasiparticle effects increase the DFT+SOC band gap by more than 1 eV.[34−36] In addition, low-dimensional structures are known to exhibit enhanced quasiparticle corrections and excitonic effects with respect to their bulk counterparts, due to the reduction of the dielectric screening.[37] Here we measured the PL response of $(C_6H_5CH_2NH_3)_4Pb_5I_{14}\cdot 2H_2O$ and observed no significant signal with respect to the noise level. Therefore, we studied the electronic structure to investigate the nature of the band gap. Since the water molecules are disordered in the structure, we considered the full structure without the water molecules, that is, $(C_6H_5CH_2NH_3)_4Pb_5I_{14}$, within GGA-DFT+SOC. Figure 3 shows the resulting band structure, which is represented more elaborately in Figure S3.

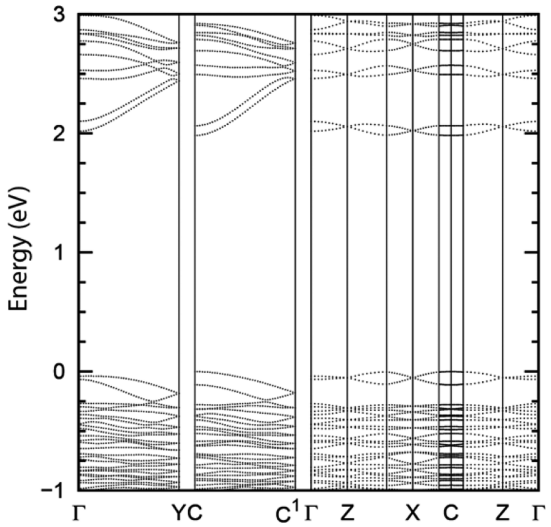

Figure 3. Band structure of $(C_6H_5CH_2NH_3)_4Pb_5I_{14}$ within DFT+SOC using the PBE functional,[27] with Γ = (0, 0, 0), X = (0.5, 0, 0), Y = (0, 0.5, 0), Z = (0, 0, 0.5), C = (0.5, 0, 0.5) or equivalent (0.5, 0, −0.5), and C^1 = (0.5, 0.5, 0.5) or equivalent (0.5, 0.5, −0.5). The coordinates denote multiples of the reciprocal lattice basis vectors $\boldsymbol{a}^*$, $\boldsymbol{b}^*$ and $\boldsymbol{c}^*$, respectively.

As can be seen in Figure 3, the band gap is direct at the C point and has the large value of 2.0 eV within DFT+SOC. We reason that this value is underestimated with respect to the real band gap due to the level of approximation used. The wide band gap can explain why no significant PL signal was observed for the $(C_6H_5CH_2NH_3)_4Pb_5I_{14}\cdot 2H_2O$ crystals. While this can be consistent with the observation that the crystals are nearly transparent in color, it does not exclude the possibility that the material can be a weak emitter due to its specific crystal structure, which might enhance nonradiative decay pathways as well. Still, the PL response differs significantly from $(C_6H_5CH_2NH_3)_2PbI_4$. The fact that the crystal structure consists of layers of inorganic PbI_6 octahedra greatly affects the size of the band gap due to the 2D confinement effect.[12,19,38] However, we find here that the connectivity between the inorganic PbI_6 octahedra within a layer has a major, additional influence on the size of the band gap. As the inorganic layers are well-separated from each other, as far as the valence and conduction bands are concerned, the electronic structure can be approximated by that of the inorganic part only.[39] We did this by taking just one $[Pb_5I_{14}]^{4-}$ ribbon from the full crystal structure. In fact, we removed the organic groups and placed the ribbons at large distances from each other such that they do not interact. Figure 4b shows that consideration of

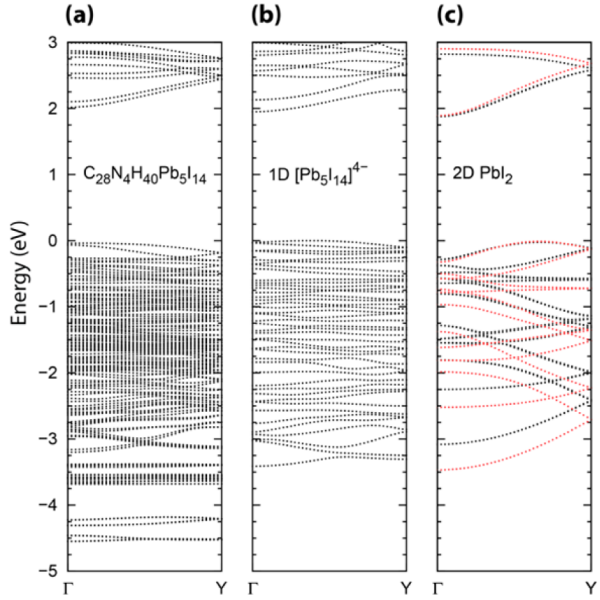

Figure 4. Comparison of the electronic band structures of (a) the full $(C_6H_5CH_2NH_3)_4Pb_5I_{14}$ crystal, (b) a single $[Pb_5I_{14}]^{4-}$ ribbon of the full crystal, and (c) an infinite 2D PbI_2 sheet created by translation of the experimental $[Pb_5I_{14}]^{4-}$ ribbon (black) and an idealized infinite 2D PbI_2 sheet with fixed Pb−I distances of 3.15 Å (red), along the common direction Γ−Y, within DFT+SOC using the PBE functional.

a single $[Pb_5I_{14}]^{4-}$ ribbon results in a relatively similar band structure to the full crystal structure. Assembling the ribbons into the complete crystal structure gives rise to a widening of the band gap on Γ−Y. The gap shifts to C, and is slightly larger than for the ribbon only. Thus, the size of the band gap is mainly determined by the inorganic slabs. Therefore, we decided to investigate the influence of edge-sharing PbI_6 octahedra in more detail. Figure 4c shows the band structure of a 2D PbI_2 sheet. We constructed this model by taking the experimental positions of the $[Pb_5I_{14}]^{4-}$ ribbons and translating them to form a 2D sheet; that is, a sheet that is infinitely extended in two dimensions. For comparison, we also made a simplified model structure in which all the Pb−I distances in the 2D PbI_2 sheet were fixed to 3.15 Å (which is a typical value for the Pb−I bond lengths in $(C_6H_5CH_2NH_3)_4Pb_5I_{14}\cdot 2H_2O$). We found that this influences the band structure but not the magnitude of the band gap. Figure 4c shows an indirect band gap of ∼1.78 eV for both models, and Figure S4 shows the band structure of the idealized 2D slab for more directions. The confinement effect involved in breaking the 2D PbI_2 sheet into $[Pb_5I_{14}]^{4-}$ ribbons is small. Therefore, our result shows that the connectivity of the PbI_6 octahedra within a layer is the key factor determining the size of the band gap, as evidenced by the significantly smaller band gap calculated for the orange counterpart $(C_6H_5CH_2NH_3)_2PbI_4$, which consists of sheets of corner-sharing octahedra rather than edge-sharing octahedra.

DOI: 10.1021/acs.inorgchem.7b01096
Inorg. Chem. 2017, 56, 8408−8414

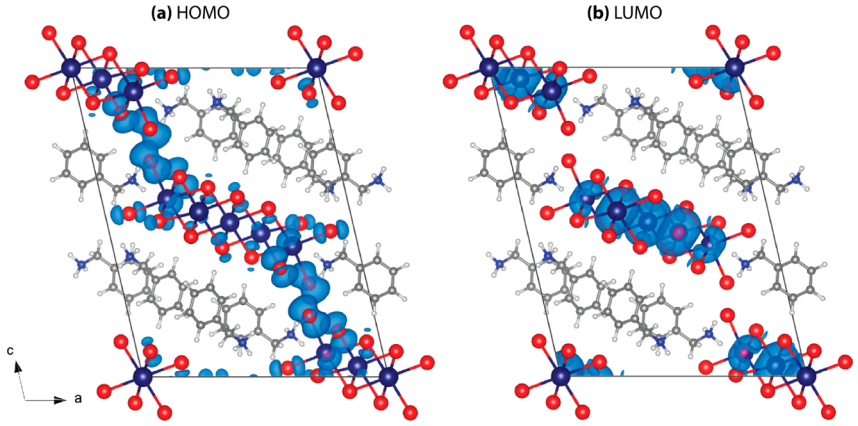

Figure 5. Spatial distributions of the electronic wave function for (a) the HOMO and (b) the LUMO at the *C* point, within DFT+SOC using the PBE functional. Shown are the pseudo charge densities augmented with soft charges near the atomic cores. Figure rendered with VESTA.[32]

To obtain a better understanding of the band structure, we also explored the effect that edge-sharing PbI_6 octahedra have on the dispersion using a tight-binding (TB) approximation. This can be found in the Supporting Information, Figures S5, S6, and Table S1.

In Figure 5 we show the spatial distributions of the electronic wave functions for the highest occupied molecular orbital (HOMO) and lowest unoccupied molecular orbital (LUMO) at the *C* point in the crystal structure of $(C_6H_5CH_2NH_3)_4Pb_5I_{14}$. Figure 5a clearly shows that the HOMO predominantly has states at the edges of the ribbons, where the terminal iodide ions are located, as can be seen in Figure 2b. Furthermore, it shows that the charges are to lesser extent distributed over the iodide ions that are part of the edge-sharing network and almost absent from the lead ions, whereas they are distributed over both parts in $(C_6H_5CH_2NH_3)_2PbI_4$.[19] Figure 5b shows that the charge is predominately distributed over the lead ions in the LUMO, similar to $(C_6H_5CH_2NH_3)_2PbI_4$.[19] Here, the distribution is largest in the middle of the inorganic ribbons.

To isolate the role of the connectivity (i.e., corner-, edge-, and face-sharing PbI_6 octahedra) on the electronic structure, we modeled several crystal structures and calculated their electronic structures. These idealized theoretical model structures exhibit fixed Pb−I distances of 3.15 Å (which is a typical value of the Pb−I bond lengths in $(C_6H_5CH_2NH_3)_4Pb_5I_{14}\cdot 2H_2O$) and fixed Pb−I−Pb angles of 180° (corner-sharing), 90° (edge-sharing), and 70.5° (face-sharing). To generalize our approach, we included three-dimensional (3D), 2D, and 1D structures. Note that corner-sharing can exist in 1D, 2D, and 3D. Edge-sharing can only occur in 1D and 2D structures, without creating corner-sharing pathways as well (see Figure S5 for further details on the 2D structure). Face-sharing can only exist in a 1D linear chain: higher-dimensional structures will also include edge- and corner-sharing, which we avoid in our models to isolate the influence of face-sharing. For all the theoretical structures, we calculated the approximate band gap within DFT, with and without SOC. The results are listed in Table 2. All of the relevant electronic band structures can be found in the Supporting Information (Figures S7−S12), together with a description of the procedure used to obtain the band gap for the charged systems.

Our results show that the band gap increases with decreasing dimensionality, which is commonly understood as a quantum confinement effect. This trend holds not only for corner-sharing PbI_6 octahedra but also for edge-sharing PbI_6 octahedra. Moreover, our results reveal another clear trend: as the connectivity varies from corner- to edge- to face-sharing (i.e., an increase in the number of I ions shared with neighboring octahedra), the band gap also increases. Thus, although the number of hopping pathways for carriers between neighboring Pb ions increases, the paths become less favorable. These trends hold for calculations that both include and exclude SOC. Furthermore, it is apparent that if the dimensionality increases, the effect of SOC is enhanced.

Table 2. Approximate Band Gaps (eV) of Theoretical[a] Model Structures with Different Connectivity and Dimensionality

	3D	2D	1D
		with spin−orbit coupling	
corner-sharing	0.10	0.94	1.82
edge-sharing		1.89	2.21
face-sharing			2.45
		without spin−orbit coupling	
corner-sharing	1.26	1.76	2.27
edge-sharing		2.48	2.61
face-sharing			2.78

[a]Calculated within DFT with and without SOC.

Notably, the size of the band gap of organic/organic hybrid materials is influenced by the interplay between the choice of metal and halide (ionic radii), structural deformations,[19−24] and the connectivity. In our study, we focused only on the aspect of connectivity, using model systems with idealized atom distances and angles, and ignored the choice of the organic cation. As a result, we directly studied the effect that connectivity has on the band gap in lead iodide systems.

CONCLUSIONS

In conclusion, we have used a layered-solution crystal-growth technique to synthesize two different benzylammonium lead iodide hybrid compounds with different ratios of constituents. Beside the known $(C_6H_5CH_2NH_3)_2PbI_4$ phase, we have characterized a new $(C_6H_5CH_2NH_3)_4Pb_5I_{14}\cdot 2H_2O$ phase consisting of ribbons of edge-sharing PbI_6 octahedra that are separated by the organic groups. Water is also incorporated into this structure. No significant photoluminescence could be measured for the latter crystal. Thus, the presence of water

DOI: 10.1021/acs.inorgchem.7b01096
Inorg. Chem. 2017, 56, 8408−8414

during synthesis can give rise to secondary phases with different structural features and undesirable optical properties. We have calculated the electronic structure of $(C_6H_5CH_2NH_3)_4Pb_5I_{14}\cdot 2H_2O$ within DFT+SOC and found a very large band gap, in agreement with our PL measurements. Moreover, by comparing the band structures of the full crystal, a single $[Pb_5I_{14}]^{4-}$ ribbon, and an extended 2D PbI_2 sheet, we found that edge-sharing of the PbI_6 octahedra is responsible for increasing the band gap relative to $(C_6H_5CH_2NH_3)_2PbI_4$, which is comprised of corner-shared octahedra. Furthermore, we modeled idealized crystal structures with different dimensionalities and octahedral connectivity and calculated their electronic structures. Our results show that the band gap increases not only with decreased dimensionality but also with increased connectivity; that is, as the connectivity of the octahedral increases from corner- to edge- to face-sharing, the band gap increases.

Our current study adds to the understanding of how the band structure is controlled by the connectivity of the inorganic lattice. Our results show that the band gap is determined by the number of iodides shared between two adjacent lead ions and is increased by higher connectivity. This understanding will facilitate direct tuning of the band gap of such materials for desired applications.

■ ASSOCIATED CONTENT

Supporting Information

The Supporting Information is available free of charge on the ACS Publications website at DOI: 10.1021/acs.inorgchem.7b01096.

photograph of crystals, asymmetric unit of $(C_6H_5CH_2NH_3)_4Pb_5I_{14}\cdot 2H_2O$, band structures of theoretical model structures with 3D, 2D, and 1D dimensionality, consisting of corner-, edge-, and face-sharing PbI_6 octahedra, tight-binding fit for edge-sharing and corner-sharing structures (PDF), and crystallographic information file of $(C_6H_5CH_2NH_3)_4Pb_5I_{14}\cdot 2H_2O$ (CIF) (PDF)

Accession Codes

CCDC 1549803 contains the supplementary crystallographic data for this paper. These data can be obtained free of charge via www.ccdc.cam.ac.uk/data_request/cif, or by emailing data_request@ccdc.cam.ac.uk, or by contacting The Cambridge Crystallographic Data Centre, 12 Union Road, Cambridge CB2 1EZ, UK; fax: +44 1223 336033.

■ AUTHOR INFORMATION

Corresponding Author

*E-mail: t.t.m.palstra@rug.nl.

ORCID

Machteld E. Kamminga: 0000-0002-3071-6996
Gilles A. de Wijs: 0000-0002-1818-0738
Remco W. A. Havenith: 0000-0003-0038-6030
Graeme R. Blake: 0000-0001-9531-7649
Thomas T.M. Palstra: 0000-0001-5239-3115

Present Address

‖University of Twente, The Netherlands.

Notes

The authors declare no competing financial interest.

■ ACKNOWLEDGMENTS

M.E.K. was supported by The Netherlands Organisation for Science NWO (Graduate Programme 2013, No. 022.005.006). We acknowledge H.-H. Fang and M. A. Loi for stimulating discussions and the measurement of the photoluminescence spectra. We thank J. Baas for discussions and technical support.

■ REFERENCES

(1) Tan, Z.-K.; Moghaddam, R. S.; Lai, M. L.; Docampo, P.; Higler, R.; Deschler, F.; Price, M.; Sadhanala, A.; Pazos, L. M.; Credgington, D.; et al. SI: Bright Light-Emitting Diodes Based on Organometal Halide Perovskite. *Nat. Nanotechnol.* **2014**, *9*, 687−692.

(2) Zhang, F.; Zhong, H.; Chen, C.; Wu, X.; Hu, X.; Huang, H.; et al. Brightly Luminescent and Color-Tunable Colloidal $CH_3NH_3X_3$ (X = Br, I, Cl) Quantum Dots: Potential Alternatives for Display Technology. *ACS Nano* **2015**, *9*, 4533−4542.

(3) Xing, G.; Mathews, N.; Lim, S. S.; Yantara, N.; Liu, X.; Sabba, D.; Grätzel, M.; Mhaisalkar, S.; Sum, T. C. Low-Temperature Solution-Processed Wavelength-Tunable Perovskites for Lasing. *Nat. Mater.* **2014**, *13*, 476−480.

(4) Zhu, H.; Fu, Y.; Meng, F.; Wu, X.; Gong, Z.; Ding, Q.; Gustafsson, M. V.; Trinh, M. T.; Jin, S.; Zhu, X.-Y. Lead Halide Perovskite Nanowire Lasers with Low Lasing Thresholds and High Quality Factors. *Nat. Mater.* **2015**, *14*, 636−642.

(5) Fang, Y.; Dong, Q.; Shao, Y.; Yuan, Y.; Huang, J. Highly Narrowband Perovskite Single-Crystal Photodetectors Enabled by Surface-Charge Recombination. *Nat. Photonics* **2015**, *9*, 679−686.

(6) Chen, Q.; Zhou, H.; Hong, Z.; Luo, S.; Duan, H.-S.; Wang, H.-H.; Liu, Y.; Li, G.; Yang, Y. Planar Heterojunction Perovskite Solar Cells via Vapor Assisted Solution Process. *J. Am. Chem. Soc.* **2014**, *136*, 622−625.

(7) Liu, D.; Kelly, T. L. Perovskite Solar Cells with a Planar Heterojunction Structure Prepared Using Room-Temperature Solution Processing Techniques. *Nat. Photonics* **2013**, *8*, 133−138.

(8) Liu, M.; Johnston, M. B.; Snaith, H. J. Efficient Planar Heterojunction Perovskite Solar Cells by Vapour Deposition. *Nature* **2013**, *501*, 395−398.

(9) Ke, W.; Fang, G.; Wan, J.; Tao, H.; Liu, Q.; Xiong, L.; Qin, P.; Wang, J.; Lei, H.; Yang, G.; et al. Efficient Hole-Blocking Layer-Free Planar Halide Perovskite Thin-Film Solar Cells. *Nat. Commun.* **2015**, *6*, 6700.

(10) Zhang, W.; Saliba, M.; Moore, D. T.; Pathak, S. K.; Hörantner, M. T.; Stergiopoulos, T.; Stranks, S. D.; Eperon, G. E.; Alexander-Webber, J. A.; Abate, A.; et al. Ultrasmooth Organic−inorganic Perovskite Thin-Film Formation and Crystallization for Efficient Planar Heterojunction Solar Cells. *Nat. Commun.* **2015**, *6*, 6142.

(11) Papavassiliou, G. C. Synthetic Three- and Lower-Dimensional Semiconductors Based on Inorganic Units. *Mol. Cryst. Liq. Cryst. Sci. Technol., Sect. A* **1996**, *286*, 231−238.

(12) Mitzi, D. B. Synthesis, Crystal Structure, and Optical and Thermal Properties of (C4H9NH3)2MI4 (M = Ge, Sn, Pb). *Chem. Mater.* **1996**, *8*, 791−800.

(13) Tanaka, K.; Takahashi, T.; Ban, T.; Kondo, T.; Uchida, K.; Miura, N. Comparative Study on the Excitons in Lead-Halide-Based Perovskite-Type Crystals $CH_3NH_3PbBr_3$ $CH_3NH_3PbI_3$. *Solid State Commun.* **2003**, *127*, 619−623.

(14) Fang, H.-H.; Raissa, R.; Abdu-aguye, M.; Adjokatse, S.; Blake, G. R.; Even, J.; Loi, M. A.; Even, J. J. Photophysics of Organic−Inorganic Hybrid Lead Iodide Perovskite Single Crystals. *Adv. Funct. Mat.* **2015**, 1−26.

(15) National Renewable Energy Laboratory. *Research Cell Efficiency Records;* National Renewable Energy Laboratory, 2015.

(16) Conings, B.; Babayigit, A.; Vangerven, T.; D'Haen, J.; Manca, J.; Boyen, H.-G. The Impact of Precursor Water Content on Solution-Processed Organometal Halide Perovskite Films and Solar Cells. *J. Mater. Chem. A* **2015**, *3*, 19123−19128.

(17) You, J.; Yang, Y. M.; Hong, Z.; Song, T.; Meng, L.; Liu, Y.; Jiang, C.; You, J.; Yang, Y. M.; Hong, Z.; et al. Moisture Assisted Perovskite

DOI: 10.1021/acs.inorgchem.7b01096
Inorg. Chem. 2017, 56, 8408−8414

Film Growth for High Performance Solar Cells Moisture Assisted Perovskite Film Growth for High Performance Solar Cells. *Appl. Phys. Lett.* **2014**, *105*, 183902.
(18) Eperon, G. E.; Habisreutinger, S. N.; Leijtens, T.; Bruijnaers, B. J.; van Franeker, J. J.; deQuilettes, D. W.; Pathak, S.; Sutton, R. J.; Grancini, G.; Ginger, D. S.; et al. The Importance of Moisture in Hybrid Lead Halide Perovskite Thin Film Fabrication. *ACS Nano* **2015**, *9*, 9380.
(19) Kamminga, M. E.; Fang, H.; Filip, M. R.; Giustino, F.; Baas, J.; Blake, G. R.; Loi, M. A.; Palstra, T. T. M. Confinement Effects in Low-Dimensional Lead Iodide Perovskite Hybrids. *Chem. Mater.* **2016**, *28*, 4554−4562.
(20) Knutson, J. L.; Martin, J. D.; Mitzi, D. B. Tuning the Band Gap in Hybrid Tin Iodide Perovskite Semiconductors Using Structural Templating. *Inorg. Chem.* **2005**, *44* (13), 4699−4705.
(21) Filip, M. R.; Eperon, G. E.; Snaith, H. J.; Giustino, F. Steric Engineering of Metal-Halide Perovskites with Tunable Optical Band Gaps. *Nat. Commun.* **2014**, *5*, 5757.
(22) Smith, M. D.; Jaffe, A.; Dohner, E. R.; Lindenberg, A. M.; Karunadasa, H. I. Structural Origins of Broadband Emission from Layered Pb-Br Hybrid Perovskites. *Chem. Sci.* **2017**, *8*, 4497−4504.
(23) Mao, L.; Wu, Y.; Stoumpos, C. C.; Wasielewski, M. R.; Kanatzidis, M. G. White-Light Emission and Structural Distortion in New Corrugated Two-Dimensional Lead Bromide Perovskites. *J. Am. Chem. Soc.* **2017**, *139*, 5210−5215.
(24) Cortecchia, D.; Neutzner, S.; Kandada, A. R. S.; Mosconi, E.; Meggiolaro, D.; De Angelis, F.; Soci, C.; Petrozza, A. Broadband Emission in Two-Dimensional Hybrid Perovskites: The Role of Structural Deformation. *J. Am. Chem. Soc.* **2017**, *139*, 39−42.
(25) Sheldrick, G. M. *SHELXL97, Program for Crystal Structure Refinement;* University of Göttingen: Germany. 1997.
(26) Hohenberg, P.; Kohn, W. Inhomogeneous Electron Gas. *Phys. Rev.* **1964**, *136*, B864−B871.
(27) Perdew, J. P.; Burke, K.; Ernzerhof, M. Generalized Gradient Approximation Made Simple. *Phys. Rev. Lett.* **1996**, *77* (18), 3865−3868.
(28) Kresse, G.; Hafner, J. *Ab Initio* Molecular Dynamics for Liquid Metals. *Phys. Rev. B: Condens. Matter Mater. Phys.* **1993**, *47*, 558−561.
(29) Kresse, G.; Furthmüller, J. Efficient Iterative Schemes for Ab Initio Total-Energy Calculations Using a Plane-Wave Basis Set. *Phys. Rev. B: Condens. Matter Mater. Phys.* **1996**, *54*, 11169−11186.
(30) Blöchl, P. E. Projector Augmented-Wave Method. *Phys. Rev. B: Condens. Matter Mater. Phys.* **1994**, *50*, 17953−17979.
(31) Kresse, G.; Joubert, D. From Ultrasoft Pseudopotentials to the Projector Augmented-Wave Method. *Phys. Rev. B: Condens. Matter Mater. Phys.* **1999**, *59*, 1758−1775.
(32) Momma, K.; Izumi, F. VESTA 3 for Three-Dimensional Visualization of Crystal, Volumetric and Morphology Data. *J. Appl. Crystallogr.* **2011**, *44*, 1272−1276.
(33) Papavassiliou, G. C.; Mousdis, G. A.; Koutselas, I. B. Some New Organic−Inorganic Hybrid Semiconductors Based on Metal Halide Unit: Structural, Optical and Related Properties. *Adv. Mater. Opt. Electron.* **1999**, *9*, 265−271.
(34) Filip, M. R.; Giustino, F. GW Quasiparticle Band Gap of the Hybrid Organic-Inorganic Perovskite $CH_3NH_3PbI_3$: Effect of Spin-Orbit Interaction, Semicore Electrons, and Self-Consistency. *Phys. Rev. B: Condens. Matter Mater. Phys.* **2014**, *90*, 245145.
(35) Filip, M. R.; Verdi, C.; Giustino, F. GW Band Structures and Carrier Effective Masses of $CH_3NH_3PbI_3$ and Hypothetical Perovskites of the Type $APbI_3$: A = NH_4, PH_4, AsH_4, and SbH_4. *J. Phys. Chem. C* **2015**, *119*, 25209−25219.
(36) Umari, P.; Mosconi, E.; De Angelis, F. Relativistic GW Calculations on $CH_3NH_3PbI_3$ and $CH_3NH_3SnI_3$ Perovskites for Solar Cell Applications. *Sci. Rep.* **2014**, *4*, 4467.
(37) Caruso, F.; Filip, M. R.; Giustino, F. Excitons in One-Dimensional van Der Waals Materials: Sb_2S_3 Nanoribbons. *Phys. Rev. B: Condens. Matter Mater. Phys.* **2015**, *92*, 125134.
(38) Cao, D. H.; Stoumpos, C. C.; Farha, O. K.; Hupp, J. T.; Kanatzidis, M. G. 2D Homologous Perovskites as Light-Absorbing Materials for Solar Cell Applications. *J. Am. Chem. Soc.* **2015**, *137*, 7843−7850.
(39) Papavassiliou, G. C.; Koutselas, I. B.; Terzis, A.; Whangbo, M.-H. Structural and Electronic Properties of the Natural. *Solid State Commun.* **1994**, *91* (9), 695−698.

DOI: 10.1021/acs.inorgchem.7b01096
Inorg. Chem. 2017, 56, 8408−8414